Available online at www.sciencedirect.com
SCIENCE DIRECT
Journal of Sound and Vibration 294 (2006) 880–893
JOURNAL OF SOUND AND VIBRATION
www.elsevier.com/locate/jsvi

Symmetric solutions for the oscillatory channel flow with arbitrary suction

Todd A. Jankowski[a], Joseph Majdalani[b,*]

[a]*Engineering Sciences and Applications Division, Los Alamos National Laboratory, MS J580, Los Alamos, NM 87545, USA*
[b]*Mechanical, Aerospace and Biomedical Engineering, The University of Tennessee (UTSI), 411 B. H. Goethert Parkway, MS-23, Tullahoma, TN 37388, USA*

Received 22 March 2005; received in revised form 21 November 2005; accepted 12 December 2005
Available online 9 March 2006

Abstract

This paper considers a porous channel in which a suction-driven flow is modulated by arbitrary levels of fluid extraction acting uniformly along its porous boundaries. When small longitudinal oscillations are enabled, a rotational wave motion is established that this study attempts to analyse. For an elongated channel, two asymptotic methods are used. The first technique is based on a two-variable multiple-scale expansion that takes into account the thin boundary layer near the wall. While retaining generality of expression, the multiple-scale procedure is carried out until a closed-form solution for the velocity field is obtained for an arbitrary mean-flow function. An alternative approach based on WKB exponentials is also employed. The WKB expansion is then pursued to arbitrary order. These asymptotic formulations are shown to agree with one another and with numeric simulations of the problem for three specific mean-flow functions.

1. Introduction

The fate of shear layers in well-established flows remains a central topic in fluid mechanics despite the considerable attention that it has received in the past. Almost every prototypical flow has undergone much scrutiny in this manner, including channel flows with porous walls. So far a number of boundary layer studies have been undertaken in the context of better understanding the multiple solutions originating from Berman's equation with wall suction or injection [1]. Examples abound and, for a thorough investigation of solution attributes that accompany suction-driven flows, the reader is referred to the survey by Zaturska et al. [2]. For multidimensional considerations, the work of Cox [3] and Taylor et al. [4] may be found useful. For injection-driven flows, one may refer to the time-dependent analyses and citations in Ref. [5]. While past studies seem to have concentrated on the existence and multiplicity of mean-flow solutions, recent focus has somewhat shifted to solutions resulting from temporal perturbations of Berman's equation.

In a previous study [5], harmonic pressure disturbances were superimposed on the injection-driven field inside a porous channel. The resulting oscillatory motion was found to exhibit rich vortical patterns displaying large penetration depths and near-wall velocity overshoot. The problem was also found to exhibit a nonlinear

*Corresponding author. Tel.: +931 393 7280; fax: +931 393 7333.
E-mail addresses: jankowski@lanl.gov (T.A. Jankowski), maji@utsi.edu (J. Majdalani).

0022-460X/$ - see front matter © 2006 Elsevier Ltd. All rights reserved.
doi:10.1016/j.jsv.2005.12.035

scaling structure due to the co-existence of several physical mechanisms within a sandwiched boundary layer. Although paradoxical at first glance, increasing viscosity led to faster vortical attenuation and reduction in the rotational depth of penetration. Furthermore, the traditionally thin viscous layer was blown off the wall to some intermediate position near the core. Under those circumstances, the penetration depth simply denoted the rotational region extending from the wall to the location of the shear layer. Obtaining asymptotic solutions required a careful application of multiple-scale and WKB theories over different ranges of the crossflow Reynolds number R.

The main purpose of this article is to extend the time-dependent study described in Ref. [5] to suction-driven flows. Despite the expected similarity with the injection-based flow analogue [5,6], it will be shown that the presence of suction significantly alters the flow character. This is due to several physical reasons. As pointed out by Catherall [7], the viscous shear layer in injection-driven flows is pushed a distance from the wall in a manner to delineate two regions of virtually inviscid flow: the first is the axial main stream, and the second consists of the permeating fluid. According to Cole and Aroesty [8], an added difficulty arises due to the inability to predict the position of the viscous layer. Our knowledge appears to be limited to the expectation that the shear layer (of order $|R|^{-1/2}$) will draw nearer to the core with successive increases in injection (cf. Ref. [9]). These features precipitate, according to Refs. [5,6], a nonlinear scaling composition that does not conform to conventional transformations which rely on linear distortions of the independent coordinate.

In the presence of suction, however, the salient mean-flow features change considerably. Streamlines switch direction as the flow heads to the closed end before it is withdrawn. Instead of being blown-off the wall, the shear layer is now formed distinctly above the porous surface. The resulting boundary layer is consistent with Prandtl's usage of the term and increases in size with viscosity. It also coincides with the rotational depth of penetration that accompanies steady and periodic flows over hard walls [10]. Unlike the injection-induced penetration depth that increases with injection, the suction-induced layer diminishes as suction levels are raised. By virtue of these mean-flow differences, one expects dissimilarities in the oscillatory wave motion and its underlying scaling structure. The same can be said of the asymptotic treatment that must accompany the resulting boundary-value problem. In view of these interesting dissimilarities, the intent of this analysis is to provide the formalism needed to obtain rigorous approximations for the oscillatory suction-driven channel flow.

Suction-induced flows were first analysed by Taylor [11] in a manufacturing process that involved running watery suspensions of fibres over porous sheets through which the fluid could be drained to form paper. Other applications have risen in the modelling of isotope separation [1], irrigation systems [12], sweat cooling [13,14], boundary layer control [15], and other filtration mechanisms. They have also been important in the modelling of the respiratory function in the lungs [16].

Since past studies have focused on steady-flow conditions, this work attempts to account for small amplitude oscillations that are often introduced by inevitable fluctuations in the suction rate. In other occasions, it is possible for the periodic motion to be induced by moving boundaries such as those arising in the modelling of the respiratory and circulatory functions in biological organisms. Regardless of the source of periodicity, this study will seek approximate solutions for the oscillatory field in the presence of uniformly distributed wall suction.

The analysis begins in Section 2 with a description of the physical geometry and system constraints. In Section 3, the governing equations are briefly presented in their general dimensional form. Subsequently, equations and variables are normalized, linearized and decomposed into steady and time-dependent sets. The temporal field is further decomposed using the momentum transport formulation. In Section 4, the multiple-scale approach is applied using two linear coordinate transformations. Next, the WKB approach is applied in Section 5. Therein, an nth order approximation is offered. A discussion is presented in Section 6 in which comparisons with numerics are reported. Finally, concluding remarks are noted in Section 7.

2. The basic flow model

A long low aspect ratio channel is considered having porous top and bottom surfaces that are separated by a distance $2h$. The side walls are assumed to be rigid and the channel width is given by w. As shown by Terrill [17], imposing the condition $w/h \geqslant 8$ enables us to simplify the problem to two space dimensions. Additionally, the solution domain is reduced in size by assuming symmetry about the channel's midsection plane. The basic

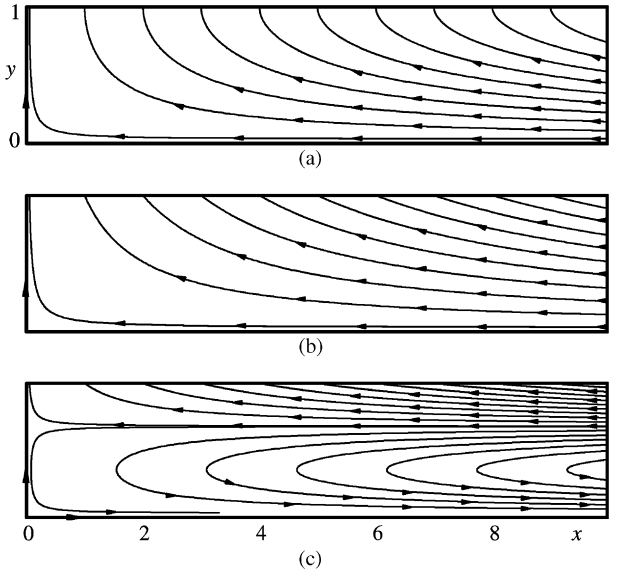

Fig. 1. System geometry showing streamlines calculated for: (a) small; (b) type I–II; and (c) type III mean-flow suction in a channel.

geometry is illustrated in Fig. 1 where a planar cross-section is shown; therein, the mean-flow streamlines are calculated based on the small and large suction solutions alluded to in Refs. [2,17]. Under these auspices, the solution domain is restricted to $0 \leqslant x^* \leqslant L$ and $0 \leqslant y^* \leqslant h$, where L is the channel length.

Under the influence of small variations in the suction rate, a channel that is closed at the head end and open at the aft end can develop longitudinal pressure oscillations of amplitude A [18]. The corresponding frequency can be specified by $\omega_s = (m - 1/2)\pi a_s/L$, where a_s refers to the stagnation speed of sound, and m is the oscillation mode shape number.

In order to simplify the forthcoming analysis, several restrictions are imposed. For example, only a laminar fluid is considered. Also, A is taken to be small in comparison with the product of stagnation pressure p_s and ratio of specific heats γ. At the outset, the dimensionless wave parameter becomes $\bar{\varepsilon} \equiv A/(\gamma p_s) \ll 1$.

Pursuant to the upcoming normalization, several nondimensional parameters will naturally emerge in the governing equations. Among them are the Mach number $M \equiv v_w/a_s$, the Strouhal number $S \equiv \omega_s h/v_w$, and the small perturbation parameter $\varepsilon \equiv 1/R = \nu/(v_w h)$. Following Ref. [5], we shall restrict our analysis to cases for which $M^2 < \bar{\varepsilon} < M \ll 1$.

3. Problem formulation

3.1. Flow decomposition

Using a similar nomenclature to that adopted in Ref. [5], the governing equations are normalized and linearized. First, spatial coordinates, velocity, pressure, density, and time are made unitless by setting

$$x = x^*/h,\ y = y^*/h,\ \mathbf{u} = \mathbf{u}^*/a_s,\ p = p^*/(\gamma p_s),\ \rho = \rho^*/\rho_s, \text{ and } t = t^*\omega_s. \tag{1}$$

Here, asterisks denote dimensional variables and ρ_s is the stagnation density. At the outset, the solution domain translates into $0 \leqslant x \leqslant l$ and $0 \leqslant y \leqslant 1$, where $l = L/h$. Second, density, pressure and velocity are perturbed in the pressure wave amplitude $\bar{\varepsilon}$. The result is

$$p(x, y, t) = p_0(x, y) + \bar{\varepsilon} p_1(x, y) \exp(-\mathrm{i}t), \tag{2}$$

$$\rho(x, y, t) = 1 + \bar{\varepsilon} \rho_1(x, y) \exp(-\mathrm{i}t), \tag{3}$$

$$\mathbf{u}(x, y, t) = M\mathbf{u}_0(x, y) + \bar{\varepsilon}\mathbf{u}_1(x, y) \exp(-\mathrm{i}t). \tag{4}$$

3.2. Leading-order decomposition

After inserting Eqs. (1)–(4) into the governing equations, one collects terms of leading order in $\bar{\varepsilon}$; one finds

$$\nabla \bullet \mathbf{u}_0 = 0, \tag{5}$$

$$M^2(\mathbf{u}_0 \bullet \nabla)\mathbf{u}_0 = -\nabla p_0 + M^2\varepsilon\left[4\nabla(\nabla \bullet \mathbf{u}_0)/3 - \nabla \times (\nabla \times \mathbf{u}_0)\right]. \tag{6}$$

Following Berman [1], a stream function can be defined such that $\Psi = -xF(y)$. This permits writing

$$\mathbf{u}_0 = u_0\hat{\mathbf{i}} + v_0\hat{\mathbf{j}} = (-xF', F). \tag{7}$$

The mean-flow momentum equation is then transformed into

$$F^{iv} + R(F'F'' - FF''') = 0, \tag{8}$$

with

$$F'(1) = F(0) = F''(0) = 0,\ F(1) = 1. \tag{9}$$

For the small suction case, Berman [1] has shown that the leading-order solution for Eq. (8) is

$$F(y) = \tfrac{1}{2}y(3 - y^2) + \mathcal{O}(R/100),\ R < 20. \tag{10}$$

Conversely, Sellars [19] has found that $F(y) = y$ is true for the large suction case. Sellars' result is also obtainable, in the limit as $R \to \infty$, from Terrill's higher-order approximation [17]

$$F(y) = \left[y - R^{-1}e^{-R(1-y)}\right]/(1 - R^{-1}) + \mathcal{O}(R^{-2}) = y + \mathcal{O}(R^{-1}),\ R \geq 20,\ \text{type I} - \text{II}. \tag{11}$$

In recent analyses, Zaturska et al. [2] have confirmed the existence of three possible solutions for $R \to \infty$. Particularly, two of their solutions labelled type I and II exhibited the same leading-order term given by Eq. (11). The type III trigonometric solution has been investigated independently by Cox and King [20] and Lu [21]. According to Lu, it could be evaluated from

$$F(y) = \begin{cases} (1 - 1/\Delta)\sin\left[\pi y/(1 - \Delta)\right]/\pi; & 0 \leqslant y \leqslant z_\varepsilon \\ (y - 1 + \Delta)/\Delta; & z_\varepsilon < y \leqslant 1; \quad z_\varepsilon = 1 - \Delta \end{cases},\ 2\pi^9\Delta\exp(R\Delta + 1) = R^7,\ R \geqslant 20,\ \text{type III}. \tag{12}$$

These mean-flow solutions will be later used to illustrate the behaviour of the conceptual function F.

3.3. Time-dependent equations

By collecting terms of order $\bar{\varepsilon}$ in the governing equations, one reaps

$$-\mathrm{i}\omega\rho_1 + \nabla \cdot \mathbf{u}_1 = -M\nabla \cdot \left(\rho_1\mathbf{u}_0\right), \tag{13}$$

$$-\mathrm{i}\omega\mathbf{u}_1 = -M[\nabla(\mathbf{u}_0 \cdot \mathbf{u}_1) - \mathbf{u}_1 \times (\nabla \times \mathbf{u}_0) - \mathbf{u}_0 \times (\nabla \times \mathbf{u}_1)] - \nabla p_1 + M\varepsilon\left[4\nabla(\nabla \cdot \mathbf{u}_1)/3 - \nabla \times (\nabla \times \mathbf{u}_1)\right]. \tag{14}$$

To make headway, the temporal field is decomposed into an acoustic, pressure-driven, irrotational wave, and a rotational, vorticity-driven, solenoidal wave. This is effectuated by letting $\mathbf{u}_1 = \hat{\mathbf{u}} + \tilde{\mathbf{u}}$, where $\nabla \times \hat{\mathbf{u}} = 0$ and $\nabla \cdot \tilde{\mathbf{u}} = 0$. This vector decomposition can be substituted into Eqs. (13) and (14) which can be subsequently solved for the acoustic velocity and pressure. Following Ref. [5], one finds

$$\hat{p} = \cos(\omega x) + \mathcal{O}(M),\ \hat{\mathbf{u}} = \mathrm{i}\sin(\omega x)\hat{\mathbf{i}} + \mathcal{O}(M), \tag{15}$$

where $\omega \equiv \omega_s h/a_s$ is the dimensionless wave frequency. Collecting terms describing the vortical set, and using Eq. (7), a solution for the axial rotational velocity is possible through the use of separation of variables. By

letting $\tilde{u} = X(x)Y(y)$, the solution becomes

$$\tilde{u}(x,y) = -\mathrm{i}\sum_{n=0}^{\infty} \frac{(-1)^n(\omega x)^{2n+1}}{(2n+1)!} Y_n(y). \tag{16}$$

Completing the solution requires determining Y_n from the boundary-value problem prescribed by

$$\varepsilon \frac{\mathrm{d}^2 Y_n}{\mathrm{d}y^2} - F\frac{\mathrm{d}Y_n}{\mathrm{d}y} + [\mathrm{i}S + (2n+2)F']Y_n = 0, \tag{17}$$

with

$$Y_n(1) = 1 \text{ and } Y_n'(0) = 0. \tag{18}$$

Here $S = \omega/M = \omega_s h/v_w$ is the Strouhal number based on the suction speed. It should be noted that Eq. (17) is identical to its counterpart arising in the injection-driven flow analogue except for the sign of F multiplying the second term. Being negative, this convective coefficient (due to the steady efflux in the normal direction) will be shown to visibly alter the flow behaviour and its required asymptotic treatment.

4. Multiple-scale analysis

Eq. (17) can be solved using a two-variable multiple-scale expansion provided the correct coordinate transformations are known. After several trials, one finds that the unique set of scales that must be resorted to consists of $y = y$ and $z = (1-y)/\varepsilon$. Note that y is the outer scale, while z is the inner variable obtained by stretching the original coordinate near the wall. Therein, a boundary layer can be expected due to the form of Eq. (17).

Insertion of the inner scale into Eq. (17) gives

$$\frac{\mathrm{d}^2 Y_n}{\mathrm{d}z^2} + F\frac{\mathrm{d}Y_n}{\mathrm{d}z} + [\mathrm{i}S + (2n+2)F']\varepsilon Y_n = 0. \tag{19}$$

By assuming that Y_n is a function of two space coordinates, the derivatives are transformed into pairs of fast and slow contributions, namely,

$$\frac{\mathrm{d}Y_n}{\mathrm{d}z} = \frac{\partial Y_n}{\partial z} - \varepsilon\frac{\partial Y_n}{\partial y},\ \frac{\mathrm{d}^2 Y_n}{\mathrm{d}z^2} = \frac{\partial^2 Y_n}{\partial z^2} - 2\varepsilon\frac{\partial^2 Y_n}{\partial y \partial z} + \mathcal{O}(\varepsilon^2). \tag{20}$$

Now letting $Y_n = Y_0 + \varepsilon Y_1 + \mathcal{O}(\varepsilon^2)$, Eq. (19) becomes

$$\frac{\partial^2 Y_0}{\partial z^2} + \varepsilon\frac{\partial^2 Y_1}{\partial z^2} - 2\varepsilon\frac{\partial^2 Y_0}{\partial y \partial z} + F\frac{\partial Y_0}{\partial z} + \varepsilon F\frac{\partial Y_1}{\partial z} - \varepsilon F\frac{\partial Y_0}{\partial y} + \varepsilon[\mathrm{i}S + (2n+2)F'](Y_0 + \varepsilon Y_1) = 0. \tag{21}$$

From Eq. (21), two equations can be segregated to determine Y_0 and Y_1. With the distinguished limit of $S \sim \varepsilon^{-1}$, the $\mathcal{O}(1)$ equation can be deduced viz.

$$\frac{\partial^2 Y_0}{\partial z^2} + F\frac{\partial Y_0}{\partial z} + \mathrm{i}S\varepsilon Y_0 = 0. \tag{22}$$

Similarly, the $\mathcal{O}(\varepsilon)$ terms can be collected into

$$\frac{\partial^2 Y_1}{\partial z^2} + F\frac{\partial Y_1}{\partial z} + \mathrm{i}S\varepsilon Y_1 = 2\frac{\partial^2 Y_0}{\partial y \partial z} + F\frac{\partial Y_0}{\partial y} - (2n+2)F'Y_0. \tag{23}$$

Solving Eq. (22) yields

$$Y_0 = A_1(y)\exp\left[\tfrac{1}{2}\left(\sqrt{F^2 - 4\mathrm{i}S\varepsilon} - F\right)z\right] + A_2(y)\ \exp\left[-\tfrac{1}{2}\left(F + \sqrt{F^2 - 4\mathrm{i}S\varepsilon}\right)z\right]. \tag{24}$$

After differentiating Eq. (24) and evaluating the right-hand side of Eq. (23), one finds that prevention of secular terms at $\mathcal{O}(\varepsilon)$ can be accomplished by imposing

$$\frac{\mathrm{d}A_1}{\mathrm{d}y} = \left[\frac{(2n+3)F'\sqrt{F^2-4\mathrm{i}S\varepsilon}-FF'}{F^2-4\mathrm{i}S\varepsilon}\right]A_1,\ \frac{\mathrm{d}A_2}{\mathrm{d}y} = \left[\frac{(2n+3)F'\sqrt{F^2-4\mathrm{i}S\varepsilon}+FF'}{4\mathrm{i}S\varepsilon-F^2}\right]A_2, \tag{25}$$

where primes denote differentiation with respect to y. After integration, the solutions of Eq. (25) can be substituted into Eq. (24). The result is

$$Y_0 = c_1\exp\left[I_1+\tfrac{1}{2}\left(\sqrt{F^2-4\mathrm{i}S\varepsilon}-F\right)(1-y)/\varepsilon\right]+c_2\exp\left[I_2-\tfrac{1}{2}\left(F+\sqrt{F^2-4\mathrm{i}S\varepsilon}\right)(1-y)/\varepsilon\right], \tag{26}$$

with

$$I_1 = \int_1^y\left[\frac{(2n+3)F'\sqrt{F^2-4\mathrm{i}S\varepsilon}-FF'}{F^2-4\mathrm{i}S\varepsilon}\right]\mathrm{d}\eta,\ I_2 = \int_1^y\left[\frac{(2n+3)F'\sqrt{F^2-4\mathrm{i}S\varepsilon}+FF'}{4\mathrm{i}S\varepsilon-F^2}\right]\mathrm{d}\eta, \tag{27}$$

where η is a dummy variable. Note that c_1 and c_2 are pure constants that can be determined from the two boundary conditions. In fact, by applying the conditions $Y_0(1)=1$ and $Y_0'(0)=0$, one concludes that $c_1=0$ and $c_2=1$. At this point, the generalized multiple-scale solution is fully realized. One finds

$$Y_n = \exp\left[I_2-\tfrac{1}{2}\left(F+\sqrt{F^2-4\mathrm{i}S\varepsilon}\right)(1-y)/\varepsilon\right]. \tag{28}$$

Note that I_2 can be carefully rearranged and integrated in a manner to yield a closed-form solution for all F. Letting $\varsigma = F$, I_2 becomes

$$I_2 = (2n+3)\int_{F(y)}^{F(1)}\frac{\mathrm{d}\varsigma}{(\varsigma^2-4\mathrm{i}S\varepsilon)^{1/2}}+\int_{F(y)}^{F(1)}\frac{\varsigma\mathrm{d}\varsigma}{\varsigma^2-4\mathrm{i}S\varepsilon}, \tag{29}$$

so that, by letting $u=\varsigma+\sqrt{\varsigma^2-4\mathrm{i}S\varepsilon}$ in the first term, one obtains

$$I_2 = \ln\left[\frac{F(1)+\sqrt{F(1)^2-4\mathrm{i}S\varepsilon}}{F+\sqrt{F^2-4\mathrm{i}S\varepsilon}}\right]^{2n+3}+\ln\left[\frac{F(1)^2-4\mathrm{i}S\varepsilon}{F^2-4\mathrm{i}S\varepsilon}\right]^{1/2}. \tag{30}$$

Recognizing that $F(1)=1$ gives

$$Y_n = \left(\frac{1+\sqrt{1-4\mathrm{i}S\varepsilon}}{F+\sqrt{F^2-4\mathrm{i}S\varepsilon}}\right)^{2n+3}\left(\frac{1-4\mathrm{i}S\varepsilon}{F^2-4\mathrm{i}S\varepsilon}\right)^{1/2}\exp\left[-\tfrac{1}{2}\left(F+\sqrt{F^2-4\mathrm{i}S\varepsilon}\right)(1-y)/\varepsilon\right]. \tag{31}$$

By substituting Eq. (31) into Eq. (16), one arrives at

$$\begin{aligned}\tilde{u}(x,y) = &-\mathrm{i}\sum_{n=0}^{\infty}\frac{(-1)^n}{(2n+1)!}\left[\frac{\omega x\left(1+\sqrt{1-4\mathrm{i}S\varepsilon}\right)}{F+\sqrt{F^2-4\mathrm{i}S\varepsilon}}\right]^{2n+1}\left(\frac{1+\sqrt{1-4\mathrm{i}S\varepsilon}}{F+\sqrt{F^2-4\mathrm{i}S\varepsilon}}\right)^2\left(\frac{1-4\mathrm{i}S\varepsilon}{F^2-4\mathrm{i}S\varepsilon}\right)^{1/2}\\ &\times\exp\left[-\tfrac{1}{2}\left(F+\sqrt{F^2-4\mathrm{i}S\varepsilon}\right)(1-y)/\varepsilon\right].\end{aligned} \tag{32}$$

At this juncture, one identifies the term inside the summation to be the MacLaurin series expansion of the sine function. This enables us to further reduce the rotational component of the axial velocity into

$$\tilde{u}(x,y) = -\mathrm{i}\left(\frac{1-4\mathrm{i}S\varepsilon}{F^2-4\mathrm{i}S\varepsilon}\right)^{1/2}\left(\frac{1+\sqrt{1-4\mathrm{i}S\varepsilon}}{F+\sqrt{F^2-4\mathrm{i}S\varepsilon}}\right)^2 \exp\left[-\left(F+\sqrt{F^2-4\mathrm{i}S\varepsilon}\right)\frac{(1-y)}{2\varepsilon}\right] \times \sin\left[\frac{\omega x\left(1+\sqrt{1-4\mathrm{i}S\varepsilon}\right)}{F+\sqrt{F^2-4\mathrm{i}S\varepsilon}}\right]. \tag{33}$$

Finally, by adding Eq. (15) the oscillatory velocity becomes

$$u_1(x,y) = \mathrm{i}\left\{\sin(\omega x) - \left(\frac{1+\sqrt{1-4\mathrm{i}S\varepsilon}}{F+\sqrt{F^2-4\mathrm{i}S\varepsilon}}\right)^2\left(\frac{1-4\mathrm{i}S\varepsilon}{F^2-4\mathrm{i}S\varepsilon}\right)^{1/2}\exp\left[-\tfrac{1}{2}\left(F+\sqrt{F^2-4\mathrm{i}S\varepsilon}\right)(1-y)/\varepsilon\right] \times \sin\left[\frac{\omega x\left(1+\sqrt{1-4\mathrm{i}S\varepsilon}\right)}{F+\sqrt{F^2-4\mathrm{i}S\varepsilon}}\right]\right\}. \tag{34}$$

Clearly, u_1 exhibits an inviscid-irrotational response followed by a wall-sensitive, visco-rotational correction that decays exponentially as $y \to 0^+$.

5. The WKB formulation

Eq. (17) can also be solved using the WKB method. Accordingly, the solution is assumed to have an exponential behaviour that is consistent with a damped wave. The corresponding expansion can be constructed from a linear combination of exponential functions of the type [22]

$$Y_n \sim \exp\left(\delta^{-1}\sum_{j=0}^{\infty}\delta^j Q_j\right), \tag{35}$$

whose derivatives exhibit the form

$$Y_n' \sim \left(\delta^{-1}\sum_{j=0}^{\infty}\delta^j Q_j'\right)\exp\left(\delta^{-1}\sum_{j=0}^{\infty}\delta^j Q_j\right),\ Y_n'' \sim \left[\delta^{-2}\left(\sum_{j=0}^{\infty}\delta^j Q_j'\right)^2 + \delta^{-1}\sum_{j=0}^{\infty}\delta^j Q_j''\right]\exp\left(\delta^{-1}\sum_{j=0}^{\infty}\delta^j Q_j\right). \tag{36}$$

By substituting Eqs. (35) and (36) into Eq. (17), one can put

$$\varepsilon\delta^{-2}\left(\sum_{j=0}^{\infty}\delta^j Q_j'\right)^2 + \varepsilon\delta^{-1}\sum_{j=0}^{\infty}\delta^j Q_j'' - F\delta^{-1}\sum_{j=0}^{\infty}\delta^j Q_j' + \mathrm{i}S + (2n+2)F' = 0 \tag{37}$$

and so, to order Q_1,

$$\varepsilon\delta^{-2}Q_0'^2 + 2\varepsilon\delta^{-1}Q_0'Q_1' + \varepsilon Q_1'^2 + \varepsilon\delta^{-1}Q_0'' + \varepsilon Q_1'' - F\delta^{-1}Q_0' - FQ_1' + \mathrm{i}S + (2n+2)F' = 0. \tag{38}$$

For the distinguished limit $S \sim \varepsilon^{-1}$, δ can be determined so that dominant terms appear at the same asymptotic order. Thus, by balancing leading terms stemming from the three main parts of Eq. (17), one obtains $\delta \sim \varepsilon$. Without loss in generality, we let $\delta = \varepsilon$ so that Eq. (38) becomes

$$\varepsilon^{-1}Q_0'^2 + 2Q_0'Q_1' + Q_0'' - F\varepsilon^{-1}Q_0' - FQ_1' + \mathrm{i}S + (2n+2)F' + \mathcal{O}(\varepsilon) = 0. \tag{39}$$

From Eq. (39), two defining equations can be deduced for Q_0 and Q_1. At $\mathcal{O}(\varepsilon^{-1})$, one collects the so-called eikonal equation [22]

$$Q_0'^2 - FQ_0' + \mathrm{i}S\varepsilon = 0. \tag{40}$$

In like fashion, the transport equation appears at $\mathcal{O}(1)$ as $Q_1' = [Q_0'' + (2n+2)F']/(F - 2Q')$. Solving Eq. (40) gives dual solutions representing left and right-travelling waves; these are

$$Q_0 = \tfrac{1}{2}\int_1^y \left(\pm\sqrt{F^2 - 4\mathrm{i}S\varepsilon} + F\right) \mathrm{d}\eta. \tag{41}$$

The leading-order WKB solution can then be constructed from the linear combination of the two possible solutions; one finds

$$Y_n = c_1 \exp\left[\tfrac{1}{2}\varepsilon^{-1}\int_1^y \left(F + \sqrt{F^2 - 4\mathrm{i}S\varepsilon}\right) \mathrm{d}\eta\right] + c_2 \exp\left[\tfrac{1}{2}\varepsilon^{-1}\int_1^y \left(F - \sqrt{F^2 - 4\mathrm{i}S\varepsilon}\right) \mathrm{d}\eta\right], \tag{42}$$

where the integration constants must be determined from the problem's boundary conditions, $Y_n(1) = 1$ and $Y_n'(0) = 0$. One concludes that $c_1 = 1$ and $c_2 = 0$. Being zero, the left-travelling wave is inconsequential. This condition is physically plausible because the current analysis does not consider wave propagation into the solid walls.

Solving at $\mathcal{O}(\varepsilon)$ can be accomplished by integrating the transport equation. One finds

$$Q_1 = -\int_1^y \left\{\left[Q_0'' + 2(n+1)F'\right]/\left(2Q_0' - F\right)\right\} \mathrm{d}\eta. \tag{43}$$

In order to evaluate Eq. (43), one must use the right-travelling wave in Eq. (41). Starting with

$$Q_0 = \tfrac{1}{2}\int_1^y \left(\sqrt{F^2 - 4\mathrm{i}S\varepsilon} + F\right) \mathrm{d}\eta, \tag{44}$$

Eq. (43) becomes

$$Q_1 = -\tfrac{1}{2}\int_1^y \left[\frac{(4n+5)F'}{\sqrt{F^2 - 4\mathrm{i}S\varepsilon}} + \frac{FF'}{F^2 - 4\mathrm{i}S\varepsilon}\right] \mathrm{d}\eta. \tag{45}$$

The complete WKB solution can then be formalized by combining both eikonal and transport solutions. One obtains

$$Y_n = \exp\left\{\tfrac{1}{2}\varepsilon^{-1}\int_1^y \left(\sqrt{F^2 - 4\mathrm{i}S\varepsilon} + F\right) \mathrm{d}\eta - \tfrac{1}{2}\int_1^y \left[\frac{(4n+5)F'}{\sqrt{F^2 - 4\mathrm{i}S\varepsilon}} + \frac{FF'}{F^2 - 4\mathrm{i}S\varepsilon}\right] \mathrm{d}\eta\right\}. \tag{46}$$

Note that the second term has been rearranged into a form that is prone to direct integration. This permits condensing Eq. (46) into

$$Y_n = \left(\frac{1 + \sqrt{1 - 4\mathrm{i}S\varepsilon}}{F + \sqrt{F^2 - 4\mathrm{i}S\varepsilon}}\right)^{2n+5/2} \left(\frac{1 - 4\mathrm{i}S\varepsilon}{F^2 - 4\mathrm{i}S\varepsilon}\right)^{1/4} \exp\left[\tfrac{1}{2}\varepsilon^{-1}\int_1^y \left(\sqrt{F^2 - 4\mathrm{i}S\varepsilon} + F\right) \mathrm{d}\eta\right]. \tag{47}$$

Using Eqs. (15), (16), and (47), the axial velocity developed from the WKB approach can be completed. This operation renders

$$u_1(x,y) = \mathrm{i}\left\{\sin(\omega x) - \left(\frac{1 + \sqrt{1 - 4\mathrm{i}S\varepsilon}}{F + \sqrt{F^2 - 4\mathrm{i}S\varepsilon}}\right)^{3/2} \left(\frac{1 - 4\mathrm{i}S\varepsilon}{F^2 - 4\mathrm{i}S\varepsilon}\right)^{1/4} \exp\left[\tfrac{1}{2}\varepsilon^{-1}\int_1^y \left(F + \sqrt{F^2 - 4\mathrm{i}S\varepsilon}\right) \mathrm{d}\eta\right] \times \sin\left[\frac{\omega x\left(1 + \sqrt{1 - 4\mathrm{i}S\varepsilon}\right)}{F + \sqrt{F^2 - 4\mathrm{i}S\varepsilon}}\right]\right\}. \tag{48}$$

Note that, unlike Eq. (34), the WKB result is given in semi-closed form. In view of its exponential term, the WKB velocity cannot be integrated in general for any F. For most mean-flow functions, numeric integration of the exponential term is necessary.

A WKB solution to any desired order may also be obtained from the higher corrections given by

$$Q_2 = -\int_1^y \left[\left(Q_1'' + Q_1'^2\right)/\left(2Q_0' - F\right)\right] \mathrm{d}\eta,\ Q_3 = -\int_1^y \left[\left(Q_2'' + 2Q_1'Q_2'\right)/\left(2Q_0' - F\right)\right] \mathrm{d}\eta \tag{49}$$

and so on. For $j \geqslant 2$, these can be reproduced from a single recurrence relation, namely,

$$Q_{j+2} = -\int_1^y \left\{ \left[Q''_{j+1} + 2Q'_1 Q''_{j+1} + \sum_{p=1}^{j-1} \left(Q'_{p+1} Q'_{j+1-p} \right) \right] / (2Q'_0 - F) \right\} \mathrm{d}\eta. \tag{50}$$

6. Discussion

6.1. Solution verification

The multiple-scale and WKB velocities given by Eqs. (34) and (48) can be compared to numerical solutions of Eqs. (16)–(18). In the process, the three characteristic functions given by Eqs. (10)–(12) can be used to describe the behaviour at small and large R. It should be noted that, for the large suction case, one may use Sellars' form [19], $F = y$ (for type I–II) to obtain closed-form asymptotic solutions and an exact solution for Eqs. (16)–(18). Under these circumstances, a numerical solution becomes confirmatory. However, both Berman's cubic polynomial, $F = \frac{1}{2}y(3 - y^2)$ [1], and Lu's type III trigonometric form, $F = (1 - \Delta^{-1}) \sin[\pi y/(1 - \Delta)]/\pi$ [21], do not permit exact solutions. A numerical outcome becomes necessary and here we use an algorithm based on Butcher's fifth-order Runge–Kutta algorithm. To ensure accuracy, a small tolerance is retained with a maximum step size of $\Delta y = 10^{-6}$. It should also be mentioned that both Berman's and Lu's solutions preclude obtaining a closed-form WKB approximation. Instead, one must rely on a quasi-analytical WKB solution requiring numerical integration of the exponential term in Eq. (48). The rotational solution for Sellars' large suction of type I–II is reported in Ref. [23]. Therein, an exact solution for Eq. (17) is derived and put in the form

$$Y_n(y) = \Phi(-n - 1 - \tfrac{1}{2}\mathrm{i}S, \tfrac{1}{2}; \tfrac{1}{2}Ry^2)\Phi^{-1}(-n - 1 - \tfrac{1}{2}\mathrm{i}S, \tfrac{1}{2}; \tfrac{1}{2}R), \tag{51}$$

so that

$$u_1(x, y) = \mathrm{i}\left[\sin(\omega x) - \sum_{n=0}^{\infty} \frac{(-1)^n (\omega x)^{2n+1}}{(2n+1)!} \frac{\Phi\left(-n - 1 - \frac{1}{2}\mathrm{i}S, \frac{1}{2}; \frac{1}{2}Ry^2\right)}{\Phi\left(-n - 1 - \frac{1}{2}\mathrm{i}S, \frac{1}{2}; \frac{1}{2}R\right)} \right], \tag{52}$$

where $\Phi(a, b; z)$ is the Kummer function [24]. In this study, Eq. (52) is used to check the validity of the numerical routine.

6.2. Error analysis

Using the exact solution as a benchmark, the maximum absolute error E_n in each of the asymptotic approximations is plotted in Fig. 2 for the type I–II mean characteristic function. Therein, both the multiple-scale and WKB solutions are systematically compared to the exact representation over a finite range of Reynolds and Strouhal numbers. Following Bosley [25], the maximum absolute error is shown versus ε for fixed S. Plotting these curves on logarithmic scales allows for the order of the error to be displayed by the

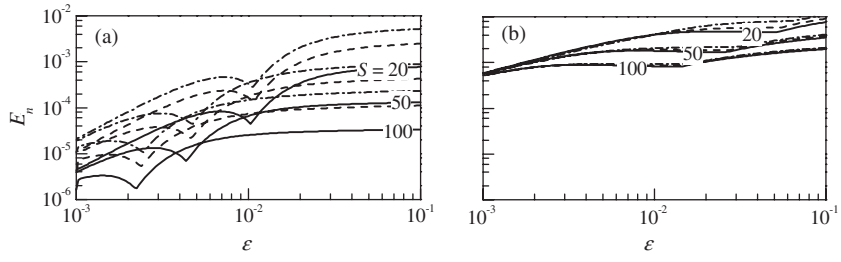

Fig. 2. Maximum absolute error between exact and asymptotic solutions using: (a) multiple-scale and (b) WKB approximations. Results correspond to mean-flow solutions of type I–II at the first three eigenvalues: $n =$ ——, 0; - - - -, 1; - - - , 2.

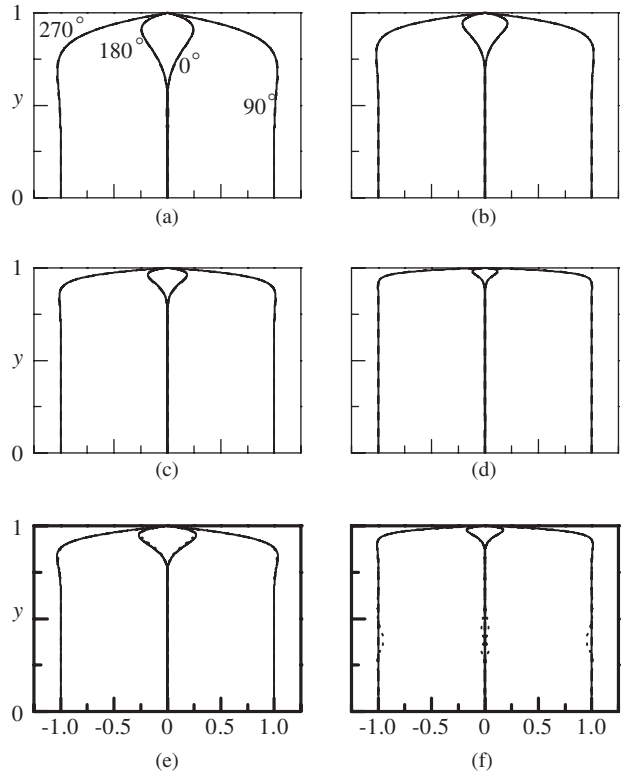

Fig. 3. Reducing viscosity or increasing suction: The oscillatory axial velocity $u_1 \exp(-it)$ is plotted at $x/l = 1$, $m = 1$, and $S = 20$. Small suction profiles are shown for: (a) $R = 5$ and (b) $R = 10$. Large suction profiles are shown with $R = 20$ for the (c) type I–II and (e) type III mean flow solutions, and with $R = 50$ for the (d) type I–II and (f) type III. Besides the results obtained via finite-differencing (FD), WKB and multiple-scale (M-S) solutions are also illustrated: ——, FD; - - - -, WKB; .....; M-S.

slope. As $\varepsilon \to 0$, the graph indicates that both approximate solutions exhibit an error of $\mathcal{O}(\varepsilon)$. This is consistent with the truncation error arising in the asymptotic treatment.

Fig. 2 also suggests that the accuracy of these approximations does not deteriorate when the $S \sim R$ condition is deviated from. In fact, both multiple-scale and WKB solutions appear to be increasingly more accurate as S is increased at constant ε, or as $\varepsilon \to 0$ at constant S. The $S \sim R$ condition remains asymptotically true because the error approaches zero the fastest when both $S \to \infty$ and $R \to \infty$.

When the standard error analysis is repeated for the type III solution, an equivalently reassuring behaviour is exhibited by the WKB solution. However, the error in the multiple-scale solution is found to be ill-behaved. The singularity detected in the multiple-scale solution for the type-III mean flow field will be discussed below.

6.3. Velocity character

Figs. 3 and 4 are used to illustrate the oscillatory suction velocity by plotting $u_1 \exp(-it)$ at four discrete timelines and a range of operating parameters. In all figures, the profiles seem to agree favourably with the classic theory of laminar periodic flows [10]. This is due to the velocity timelines being representative of a spatially damped wave propagating in time. The travelling wave exhibits a large inviscid core that stretches across the symmetry plane. It also exhibits a rotational boundary layer in the direct vicinity of the wall. At the wall ($y = 1$), the no-slip condition is satisfied. The thickness of the rotational region is also comparable in size to the Stokes layer [10].

In Fig. 3, both multiple-scale and WKB solutions are used to illustrate the effect of increasing the Reynolds number while keeping all other parameters constant. For the smallest suction level of $R = 10$, the relative

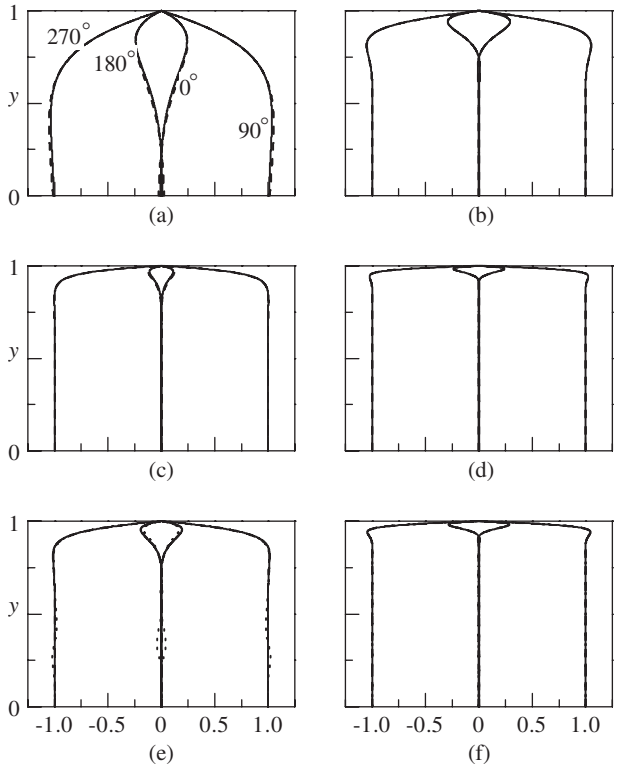

Fig. 4. Increasing frequency: the oscillatory axial velocity $u_1 \exp(-it)$ is plotted at $x/l = 1$ and $m = 1$. Parameters used for the small suction profiles are $R = 3$ with: (a) $S = 10$ and (b) $S = 100$. For large suction $R = 30$. The mean-flow solutions of types I–II are shown with (c) $S = 10$ and (d) $S = 100$. The type III solution is illustrated with (e) $S = 10$ and (f) $S = 100$. The finite-difference (FD), WKB, and multiple-scale (M-S) solutions are shown: ——, FD; - - - -, WKB;.....; M-S.

effect of viscosity is the most appreciable. In this case, the rotational layer penetrates deeper into the channel than at higher suction levels. For the same physical reason, a relatively larger overshoot is observed near the wall. As suction is increased, the relative importance of viscous effects diminishes. Profiles drawn at increasing Reynolds numbers show that the rotational layer undergoes progressive compressions. With successive increases in suction, the companion overshoot diminishes as well. These physical characteristics can be explained in light of the asymptotic solutions that have been derived. For example it is possible to infer from Eq. (34) that the rotational amplitude must be strongly influenced by $\exp\left[-\frac{1}{2}R(1-y)\right]$. Thus, as the core is approached, the wave amplitude decays more rapidly at bigger R. Since the wave amplitude prescribes the boundary layer envelope, a thinner boundary layer ensues. The overshoot is similarly affected since a smaller rotational contribution near the wall leads to a smaller total velocity.

The influence of the oscillation frequency is examined in Fig. 4 where the velocity is shown at small and large Strouhal numbers. Overall, it can be seen that an order of magnitude increase in frequency (for either small or large suction) causes a reduction in penetration depth and an increase in overshoot. This effect can be ascribed to the reduced spatial wavelength which, from Eq. (34), is inversely proportional to the Strouhal number. For larger S, the correspondingly shorter wavelength allows for the pairing between acoustic and rotational wave components to take place closer to the wall. Since the rotational velocity is larger near the wall, the vortical excess is appreciably higher when high frequency oscillations are present. When this supplemental contribution is added to the inviscid amplitude, a slightly larger overshoot is observed. The increased frequency also leads to faster particle reversals and, therefore, to more rapid viscous dissipation of the rotational disturbances born at the surface. This mechanism explains the reduced depth of penetration at higher frequencies.

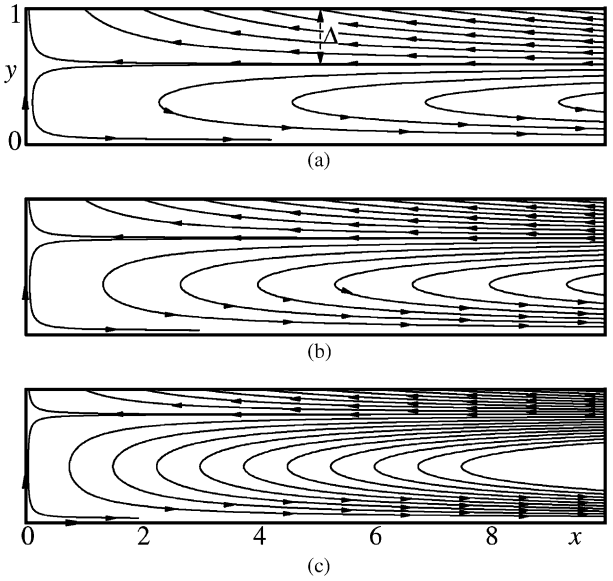

Fig. 5. Streamline patterns corresponding to the type III characteristic function exhibiting sharp flow turning near the wall and complete reversal near the core ($0<y<1-\Delta$). The figures correspond to: (a) $R=30$; (b) $R=60$; and (c) $R=120$. Note that $\Delta\to 0$ as $R\to\infty$.

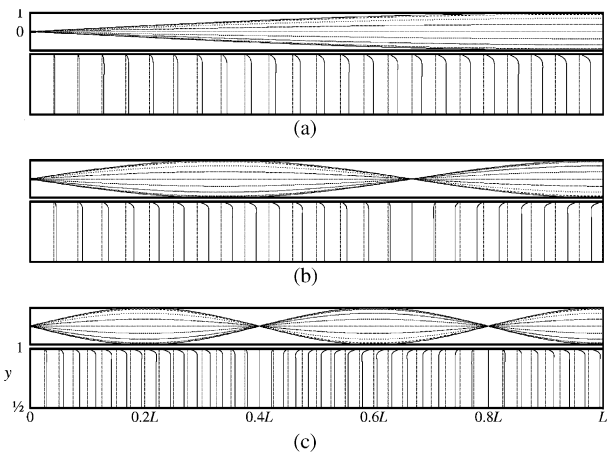

Fig. 6. For the first three oscillation modes, the modulus of $u_1\exp(-\mathrm{i}t)$ is plotted at evenly spaced locations along the channel's length. Also shown are the corresponding acoustic velocity mode shapes (top part). Using the type-III mean-flow function, the effect of increasing the oscillation mode number is captured by fixing the suction Reynolds number at $R=30$, and varying the Strouhal number according to $S=30m$, where (a) $m=1$, (b) $m=2$ and (c) $m=3$. Note that the smallest disturbances take place at the interior velocity nodes for $x/l=n/(m-1/2); n<m$.

When the multiple-scale solution is used in conjunction with the type-III function, a noticeable discrepancy is seen by comparison with the numerical or WKB predictions. This discrepancy is more significant at smaller values of R. The singularity in the multiple-scale solution can be attributed to the failure of linear distortions of the coordinate in regions where $F<0$, namely, for $0<y<1-\Delta$. In this interval, the flow direction switches such that fluid layers are pushed away from the porous surface as in the injection-driven problem (see Fig. 5). The convection of the mean flow layers away from the porous wall leads to a nonlinear scaling structure that cannot be captured by the linear coordinate transformation used here. As illustrated in Fig. 5, complex streamline patterns are formed at different suction levels. The sign reversal in the normal velocity mimics the

effect of injection, a mechanism that has been proven to exhibit nonlinear scales where $F<0$ (see Ref. [5]). This region of nonuniformity for the type-III multiple-scale solution expands with increasing R. It is narrowest near $R=13.7$ where the largest value of $\Delta=0.5108$ can be obtained.

The spatial evolution of the type-III oscillatory solution is displayed in Fig. 6 at the fundamental and first two harmonic mode shapes. This is accomplished by plotting the modulus of the time-dependent wave at equally spaced intervals along the length of the closed-open channel using either the numerical or the equivalent WKB solution. For each value of m, the amplitude of the inviscid response is superposed in order to illustrate the strong connection between the pressure-driven, acoustic amplitude, and the rotational, boundary-driven component. Most notably, both acoustic and rotational wave amplitudes are suppressed at the downstream locations of acoustic velocity nodes. This is contrary to the effect observed in the injection-driven flow analogue wherein rotational disturbances are spread deeper into the core and throughout the chamber. Here vortices are strictly confined to the thin boundary layer above the wall. A similar spatial evolution is displayed by the other cases of F.

7. Concluding remarks

This study provides two general asymptotic forms of the oscillatory suction flow in a porous channel. Both multiple-scale and WKB expansions coincide in predicting the form of the rapidly damped wave using Berman's and Sellar's type I–II mean flow solutions. For Lu's type-III solution, the multiple-scale solution based on linear stretching of the coordinate becomes inadequate over the interval in which the flow reverses. This result confirms the need for a nonlinear scaling transformation emphasized in the injection-driven flow problem [5]. The oscillatory wave bears a striking resemblance to the Stokes profile in exhibiting small penetration depths and near-wall overshoot factors. Its advantage lies in its inclusion of two space dimensions that take into account the finite length of the channel. The solution also accounts for different oscillation mode shapes and end-wall boundary conditions. Since the current study is carried out for a closed-open channel, the same can be extended to other geometric shapes and acoustic configurations. Another interesting finding is the identification of the inner scale that can lead to a uniformly valid solution for suction-dominated flows. The conventional presence of a boundary layer near the wall has, to some extent, enabled us to apply a linear distortion of the normal coordinate y. This linear stretching has provided the necessary resolution to achieve closure in the two-variable multi-scale expansion associated with both Berman's and Sellar's type I–II mean flow solutions for which $F\geq 0$. Similar linear transformations of the independent variable were not useful in the injection-driven flow analogue [5,6]. Previously, nonlinear transformations and a generalized-scaling technique had to be pursued in order to identify the multi-scale structure. In the current study, the multiple-scale solution has led to an unconditionally closed-form expression for an arbitrary mean-flow function $F\geq 0$. Its simplicity has also enabled us to understand or confirm the observed dependence on several operating parameters. The WKB technique, on the other hand, has been instrumental in providing higher approximations to any desired order. In comparison to the injection-driven problem, the rotational effects are much smaller here. Suction acts to suppress the spreading of unsteady vorticity by convective withdrawal at the wall. In both physical settings, increasing the frequency or Strouhal number leads to smaller penetration depths and larger overshoot factors. However, a contrasting behaviour accompanies changes in viscosity. In studies concerned with injection [5,6], higher viscosities have induced shorter depths of penetration. This is due to the wave decay being controlled by the damping parameter $\xi=\nu\omega^2 h/v_w^3$. At present, the damping role is transferred to the suction Reynolds number $R=v_w h/\nu$. A reversal in the role of viscosity is precipitated. Another dissimilarity lies in the size of the viscous layer. As confirmed by the distinguished limits demanded by WKB formalism, the thickness of the inner layer decreases from $\delta=(-R)^{-1/2}$ for injection to $\delta=R^{-1}$ for suction. Thus, for the same physical properties and absolute speed $|v_w|$, a thinner inner layer is formed during suction. Apparently, more rapid changes in gradually smaller distances are distinguishing attributes of both mean and oscillatory components of suction-driven flows. This behaviour is commensurate with the increased stiffness that has often prevented former investigations from exploring higher suction Reynolds numbers (see Ref. [26] or, recently, Ref. [27]). While the increased stiffness with R requires progressively higher mesh resolutions during numerical integrations, the physical models presented heretofore must remain hypothetical until corroborated by laboratory experiments.

Acknowedgement

This work was sponsored by the National Science Foundation through Grant no. CMS-0353518.

References

[1] A.S. Berman, Laminar flow in channels with porous walls, *Journal of Applied Physics* 24 (1953) 1232–1235.
[2] M.B. Zaturska, P.G. Drazin, W.H.H. Banks, On the flow of a viscous fluid driven along a channel by suction at porous walls, *Fluid Dynamics Research* 4 (1988) 151–178.
[3] S.M. Cox, Two-dimensional flow of a viscous fluid in a channel with porous walls, *Journal of Fluid Mechanics* 227 (1991) 1–33.
[4] C.L. Taylor, W.H.H. Banks, M.B. Zaturska, P.G. Drazin, Three-dimensional flow in a porous channel, *Quarterly Journal of Mechanics and Applied Mathematics* 44 (1991) 105–133.
[5] J. Majdalani, The oscillatory channel flow with arbitrary wall injection, *Journal of Applied Mathematics and Physics* 52 (2001) 33–61.
[6] J. Majdalani, T.S. Roh, The oscillatory channel flow with large wall injection, *Proceedings of the Royal Society* 456 (2000) 1625–1657.
[7] D. Catherall, K. Stewartson, P.G. Williams, Viscous flow past a flat plate with uniform injection, *Proceedings of the Royal Society, London* 284 (1965) 370–396.
[8] J.D. Cole, J. Aroesty, The blowhard problem-inviscid flows with surface injection, *International Journal of Heat and Mass Transfer* 11 (1968) 1167–1183.
[9] R.M. Terrill, Laminar flow in a uniformly porous channel with large injection, *The Aeronautical Quarterly* 16 (1965) 323–332.
[10] N. Rott, *Theory of Time-Dependent Laminar Flows*, Princeton University Press, Princeton, NJ, 1964.
[11] G.I. Taylor, Fluid flow in regions bounded by porous surfaces, *Proceedings of the Royal Society, London* 234 (1956) 456–475.
[12] A.S. Berman, Laminar flow in an annulus with porous walls, *Journal of Applied Physics* 29 (1958) 71–75.
[13] S.W. Yuan, *Cooling by Protective Fluid Films*, Princeton University Press, Princeton, NJ, 1959.
[14] Y. Peng, S.W. Yuan, Laminar pipe flow with mass transfer cooling, *Journal of Heat Transfer* 87 (1965) 252–258.
[15] B.M. Leadon, *The Status of Heat Transfer Control by Mass Transfer for Permanent Surface Structures*, Prentice-Hall, Inc., Englewood Cliffs, NJ, 1962.
[16] M.Y. Jaffrin, A.H. Shapiro, Peristaltic pumping, *Annual Review of Fluid Mechanics* 3 (1971) 13–36.
[17] R.M. Terrill, Laminar flow in a uniformly porous channel, *The Aeronautical Quarterly* 15 (1964) 299–310.
[18] P.M. Morse, K.U. Ingard, *Theoretical Acoustics*, McGraw-Hill, New York, 1968.
[19] J.R. Sellars, Laminar flow in channels with porous walls at high suction Reynolds numbers, *Journal of Applied Physics* 26 (1955) 489–490.
[20] S.M. Cox, A.C. King, On the asymptotic solution of a high-order nonlinear ordinary differential equation, *Proceedings of the Royal Society, London* 453 (1997) 711–728.
[21] C. Lu, On the asymptotic solution of laminar channel flow with large suction, *SIAM Journal on Mathematical Analysis* 28 (1997) 1113–1134.
[22] C.M. Bender, S.A. Orszag, *Advanced Mathematical Methods for Scientists and Engineers*, McGraw-Hill, New York, 1978.
[23] T.A. Jankowski, J. Majdalani, Acoustical and vortical interactions inside a channel with wall suction, in: sixth AIAA/CEAS Aeroacoustics Conference and Exhibit, Paper No. 2000-1988, Lahaina, HA, June 2000.
[24] M. Abramowitz, I.A. Stegun, *Handbook of Mathematical Functions*, National Bureau of Standards, New York, 1964.
[25] D.L. Bosley, A technique for the numerical verification of asymptotic expansions, *SIAM Review* 38 (1996) 128–135.
[26] S.W. Yuan, Further investigation of laminar flow in channels with porous walls, *Journal of Applied Physics* 27 (1956) 267–269.
[27] J.R. King, S.M. Cox, Asymptotic analysis of the steady-state and time-dependent Berman problem, *Journal of Engineering Mathematics* 39 (2001) 87–130.